Optical properties of guided-mode resonant gratings with linearly varying period

Dmitry A. Bykov [ORCID],[*] Evgeni A. Bezus [ORCID], Andrey A. Morozov [ORCID], Vladimir V. Podlipnov [ORCID], and Leonid L. Doskolovich [ORCID]

Image Processing Systems Institute—Branch of the Federal Scientific Research Centre "Crystallography and Photonics"
of Russian Academy of Sciences, 151 Molodogvardeyskaya Street, Samara 443001, Russia
and Samara National Research University, 34 Moskovskoye Shosse, Samara 443086, Russia

Guided-mode resonant gratings with spatially varying parameters are widely used as linear variable optical filters, and their behavior is often described using the so-called local periodic approximation, in which the structure is locally replaced by a strictly periodic grating with the period coinciding with the "local" period at the considered point. In this work, we investigate the optical properties of guided-mode resonant gratings with the period linearly varying along the periodicity direction. Using full-wave numerical simulations, we show that when the period change rate is relatively high (about 0.5–1 μm/mm for the considered structures), the local periodic approximation becomes inapplicable, and the linewidth and the line shape of the resonances depend significantly on the period change rate. We qualitatively explain the appearance of an asymmetric non-Fano line shape with secondary maxima by analyzing the local photonic band structure of the studied varying-period gratings. For a more accurate description of such gratings, we develop a spatiotemporal coupled-mode theory, the predictions of which are in good agreement with the rigorous numerical simulation results. The validity of the derived theoretical model is additionally confirmed by a proof-of-concept experiment with a varying-period guided-mode resonant grating. The obtained results may find application in the design of compact linear variable filters based on resonant gratings with spatially varying parameters.

I. INTRODUCTION

Over the past decade, much attention has been paid to the study of resonant effects in nanophotonic structures [1,2] due to both fundamental interest and numerous potential applications in optical filters and spectrometers, chemical and biological sensors, laser and photovoltaic devices, etc. [1]. One of the most comprehensively studied types of resonant photonic structures is constituted by diffraction gratings. Despite a long history [3–6], such structures continue to attract great research interest due to a wide range of extraordinary optical effects exhibited under resonant conditions [7–9].

One of the most important applications of resonant diffraction gratings is found in the problem of spectral filtering of light. For this purpose, single-layer subwavelength dielectric gratings as well as two-layer structures consisting of a grating located on the surface of a dielectric slab waveguide are widely used [10–14]. The optical properties of such structures, namely, narrow peaks and dips in the reflection and transmission spectra, have a resonant nature and are associated with the excitation of quasiguided modes in the grating or in the waveguide layer.

When creating spectrometric systems, the problem of dividing the incident radiation into a large number of spectral channels arises. An efficient approach to the creation of spectral filters for such systems is the use of resonant diffractive structures, in which one or several parameters change in

the plane of the structure. This enables filtering different wavelengths in different regions of the filter. Usually, the filtered wavelength changes linearly across a certain spatial dimension of the filter; such structures are referred to as linear variable filters (LVFs). The most well-known LVF type is based on multilayer phase-shifted Bragg gratings with a wedged central ("defect") layer [15–19].

Resonant diffraction gratings with one or several parameters, which change in the direction of the periodicity or in the perpendicular direction, constitute another promising type of LVFs [20–41]. One of the advantages of such gratings is that their thickness is comparable with the incident wavelength since they consist of only one (the diffraction grating itself) or two (grating and waveguide) layers. They are also relatively easy to fabricate since for their creation, simple and cheap methods of interference lithography [20,21] and ion-beam etching with a mask [19,20] can be used. In addition to the spectrometric applications, the gratings with spatially varying parameters are also promising for use as refractive index sensors [29,33], biosensors [36,39], and torque sensors [27].

Most often, the period of the diffraction grating is used as the varying parameter [24–32]. In the vast majority of cases, the rate of change in the period is very small and, as a rule, lies in the range 5–50 nm/mm (i.e., 0.005–0.05 μm/mm). Note that the period in these works does not exceed the wavelength of the incident light, which makes such gratings different from the so-called varied line-space (VLS) gratings [42]. In [33–35], the thickness of the waveguide layer changes (the rate of change is from 0.7 to 8 nm/mm). In [22,23], the thickness of the diffraction grating is used as the varying

*bykovd@gmail.com

parameter (with variation rates of 1.1–3.3 nm/mm). In [36], the duty cycle of the grating is changed. In some works, two parameters are varied simultaneously: the period and waveguide layer thickness in [37–40] and the period and grating height in [41]. In the mentioned papers, the varying parameter (or parameters) changes rather slowly. For the description of such "slowly varying" structures, it is usually sufficient to use the so-called local periodic approximation (LPA), in which a structure with varying parameters is locally approximated by an infinite periodic structure with parameters coinciding with the parameters of the initial structure at the current point. At the same time, the design of compact filters requires the development of a theoretical model describing resonant optical properties and filtering performance of varying-period structures at higher period change rates, where the LPA is no longer applicable. Such a theory, on the one hand, would enable achieving an optimal trade-off between the spectral resolution, the width of the working spectral range, and the geometrical dimensions of the filter and, on the other hand, would make it possible to estimate the limits of applicability of the LPA. In this regard, it is important to note that the overwhelming majority of works devoted to grating-based linear variable filters are either purely experimental [20–31,33–39,41] or purely numerical [32,40], and for structures of this type, no theory has been developed to describe, in particular, the broadening, change in the line shape, and shift of the spectral peaks caused by the spatial variation of the parameters of the structure.

In the present work, we theoretically, numerically, and experimentally investigate varying-period guided-mode resonant gratings with relatively high period change rates reaching 1 μm/mm. In Sec. II, we briefly discuss strictly periodic guided-mode resonant gratings and introduce the geometry of the studied structures with linearly varying period. In Sec. III, we present the results of the numerical simulations of the varying-period structures. Section IV provides a qualitative explanation of the appearance of non-Fano resonance line shapes with secondary maxima in terms of the local photonic band structure. In Sec. V, we derive a coupled-mode theory (CMT) describing the resonant optical properties of guided-mode resonant gratings with a spatially varying period. Section VI presents the results of a proof-of-concept experiment confirming the validity of the developed theoretical model. Section VII concludes the paper.

II. GUIDED-MODE RESONANT GRATINGS WITH LINEARLY VARYING PERIOD

The geometry of the investigated structure is schematically depicted in Fig. 1(a). The structure consists of a binary diffraction grating with height h_{gr} placed on top of a dielectric slab waveguide with thickness h_{wg}. The period of the grating $d(x)$ varies in the direction of the x axis. Although such a structure is not periodic, for the sake of convenience, we will still refer to this direction as the periodicity direction.

Before studying the optical properties of a structure with varying period, let us briefly revisit the strictly periodic case, for which $d(x) = d_0 = $ const [Fig. 1(b)]. We consider an example with the following parameters: grating period $d_0 = $
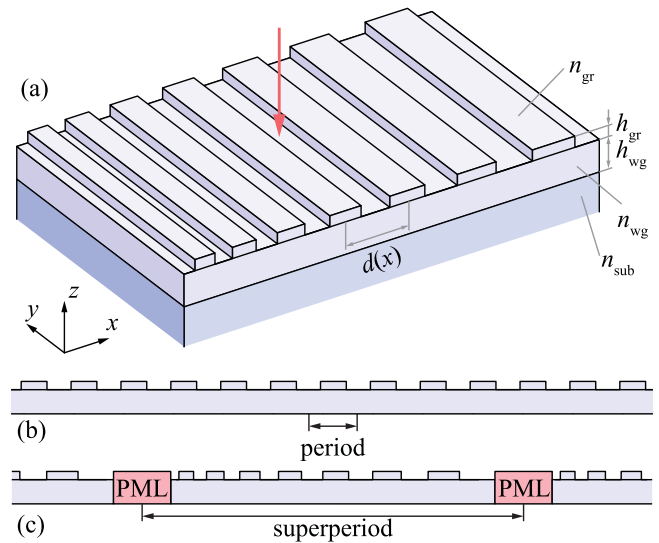

FIG. 1. (a) Geometry of the considered varying-period structure. (b) Geometry of a strictly periodic grating used for the local periodic approximation of the varying-period structure. (c) Simulation supercell of the varying-period structure with adjacent superperiods separated by perfectly matched layers (PMLs).

195 nm, ratio of the ridge width to the grating period (fill factor) $f = 0.9$, grating height $h_{gr} = 30$ nm, waveguide layer thickness $h_{wg} = 50$ nm, refractive index of the grating and the waveguide layer $n_{gr} = n_{wg} = 3.5$, and refractive indices of the superstrate and substrate $n_{sup} = 1$ and $n_{sub} = 1.5$, respectively.

At normal incidence of a transverse-electric- (TE-) polarized plane wave, this structure exhibits a resonant reflectance peak at $\lambda = 544$ nm (see the inset in Fig. 2). At this wavelength, the magnitude of the in-plane wave-vector components of the positive and negative first diffraction orders matches

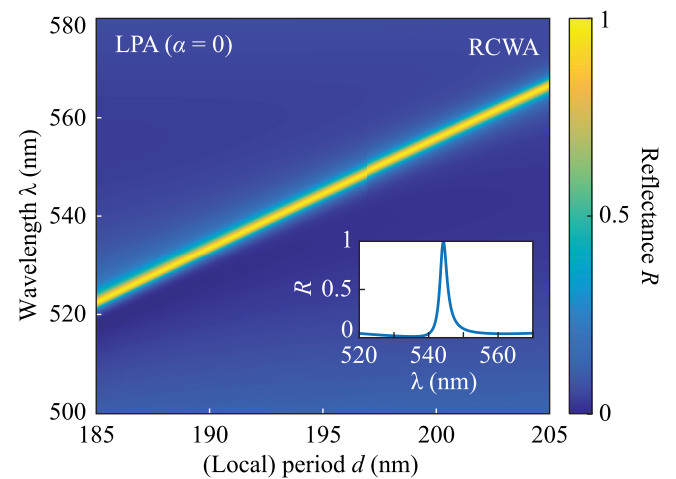FIG. 2. Reflectance R of a strictly periodic grating vs its period and wavelength of a normally incident plane wave calculated using RCWA. The plot can also be regarded as the reflected field distributions over a varying-period structure at different wavelengths calculated using the local periodic approximation ($\alpha = 0$). The inset shows the reflectance spectrum of a grating with period $d_0 = 195$ nm.

the wave number of the guided mode of the slab waveguide. Therefore, the resonance arises due to the excitation of this eigenmode. Since the reflectance peak appears on a low background, this structure can be utilized as a narrow-band spectral filter. The spectral position of the reflectance peak changes almost linearly with a change in the period of the structure. This is illustrated by Fig. 2 showing the reflectance spectra vs the grating period d. The reflectance was calculated using the rigorous coupled-wave analysis (RCWA; also referred to as the Fourier modal method) [43,44].

For applications in optical filtering and sensing, it is important to design a structure with linearly varying period [Fig. 1(a)] providing the filtering of different wavelengths at different spatial positions along the periodicity direction. As was mentioned in the Introduction, such structures are usually referred to as linear variable filters. As in the case of fixed-period gratings, the filtering properties of such structures have a resonant nature (in contrast to the VLS gratings [42], the optical properties of which are determined by a change in the direction of a nonspecular diffraction order).

In this work, we will consider the following linear period variation law:

$$d(x) = d_0 + \alpha x, \tag{1}$$

where $d_0 = 195$ nm is the central period and α defines the period change rate. Note that $d(x)$ in Eq. (1) is the local period, which is, roughly speaking, the distance between the centers of two adjacent grating ridges [see Fig. 1(a)].

Let us design a structure with the local period varying according to Eq. (1). To do this, we define the dielectric permittivity inside the unit cell of the grating layer using the function $\varepsilon(t)$, which is periodic with unit period [$\varepsilon(t + 1) = \varepsilon(t)$] and, at $t \in [0, 1]$, reads

$$\varepsilon(t) = \begin{cases} n_{\mathrm{gr}}^2, & t \leqslant f, \\ n_{\mathrm{sup}}^2, & t > f. \end{cases}$$

Therefore, the grating with a fixed period d_0 is described by the function $\varepsilon(x/d_0)$. Now, let us choose the argument of $\varepsilon(t)$ to be $\varepsilon(x/D(x))$ and find such a function $D(x)$, so that the *local* period of the varying-period structure agrees with Eq. (1). Counterintuitively, the "naive" approach of using $D(x) = d(x)$ turns out to be wrong. Indeed, the *local* period can be found by analyzing how fast the argument of the function ε is changing, i.e., by evaluating the derivative of $x/D(x)$, which should be equal to the local period inverse. By writing this condition, we arrive at the following differential equation:

$$\frac{1}{D(x)} - x \frac{D'(x)}{D(x)^2} = \frac{1}{d(x)}. \tag{2}$$

Using Eq. (1) and requiring $\lim_{x \to 0}[x/D(x)] = 0$, we obtain the following solution:

$$D(x) = \frac{\alpha x}{\ln\left(1 + \alpha \frac{x}{d_0}\right)}. \tag{3}$$

Since $D(x) = d_0 + \frac{\alpha x}{2} + O(\alpha^2)$, the period should change approximately two times slower than in the naive approach assuming $D(x) = d(x)$.

Summarizing this section, we have shown that the function $\varepsilon(x/D(x))$ with $D(x)$ given by Eq. (3) defines the geometry

of the structure with the linearly varying local period $d(x)$ [Eq. (1)].

III. NUMERICAL SIMULATION

Having determined the geometry of the varying-period grating, let us now move to the discussion of its optical properties. When considering such structures as optical filters, one is usually interested in the reflectance and transmittance at different points of the structure (along its periodicity direction) and different wavelengths [20,21,29,30,33,38]. When the period change rate α is sufficiently small, at each point of the varying-period grating, we can replace it with a strictly periodic one with the period equal to the local period of the investigated varying-period structure. Under this local periodic approximation, we arrive at the very same Fig. 2 with the period d being the local period of the investigated structure. When, however, the value of α is of the order of 10^{-4} (0.1 μm/mm) or greater, the LPA ceases to be valid, and a more elaborate theoretical description is required. In order to demonstrate this, let us simulate the whole varying-period structure.

As in the previous section, for the simulation, we used the rigorous coupled-wave analysis [43,44]. However, since the RCWA is aimed at simulating strictly periodic diffractive structures, the following superperiod (supercell) approach had to be used. The considered varying-period structure, consisting of a certain large, but finite, number of periods, was artificially periodized along the x axis. The adjacent artificial periods (superperiods) were separated by absorbing perfectly matched layers (PMLs) in order to eliminate the optical interaction between them [see Fig. 1(c)]. To estimate the reflectance of the structure, we simulated the diffraction of a normally incident TE-polarized plane wave and calculated the reflected field distribution $|E_y|^2$ along a straight horizontal line located 170 nm above the structure. The described simulation was performed for wavelengths from the spectral range of interest, 500–580 nm.

The simulation results are presented in Figs. 3(a)–3(c), which correspond to three different period change rates α: 0.2, 0.5, and 1 μm/mm, respectively. In the simulations, the superperiod contained a segment of the varying-period structure with the local periods ranging from 185 to 205 nm. At the considered period change rates, this leads to the following sizes of the simulated structures: $W = 100\,\mu$m [Fig. 3(a)], $W = 40\,\mu$m [Fig. 3(b)], and $W = 20\,\mu$m [Fig. 3(c)]. Therefore, the total superperiod of the simulated structure, which also includes the PML regions, exceeds 200λ, which requires the use of about $2 \times 1000 + 1$ Fourier harmonics in the RCWA. Such a simulation can be performed on a modern desktop PC; nevertheless, let us mention that if at larger superperiods, the memory and time requirements of the conventional RCWA become prohibitively large, the contrast-field formulation of the RCWA can be utilized [45,46].

It is evident from Figs. 3(a)–3(c) that the investigated varying-period structures exhibit pronounced reflectance peaks with the spatial position depending on the incident wavelength. In order to discuss the shape of the resonant peaks in more detail, let us examine the vertical cross sections of the reflectance plots shown in Figs. 2 and 3(a)–3(c). The
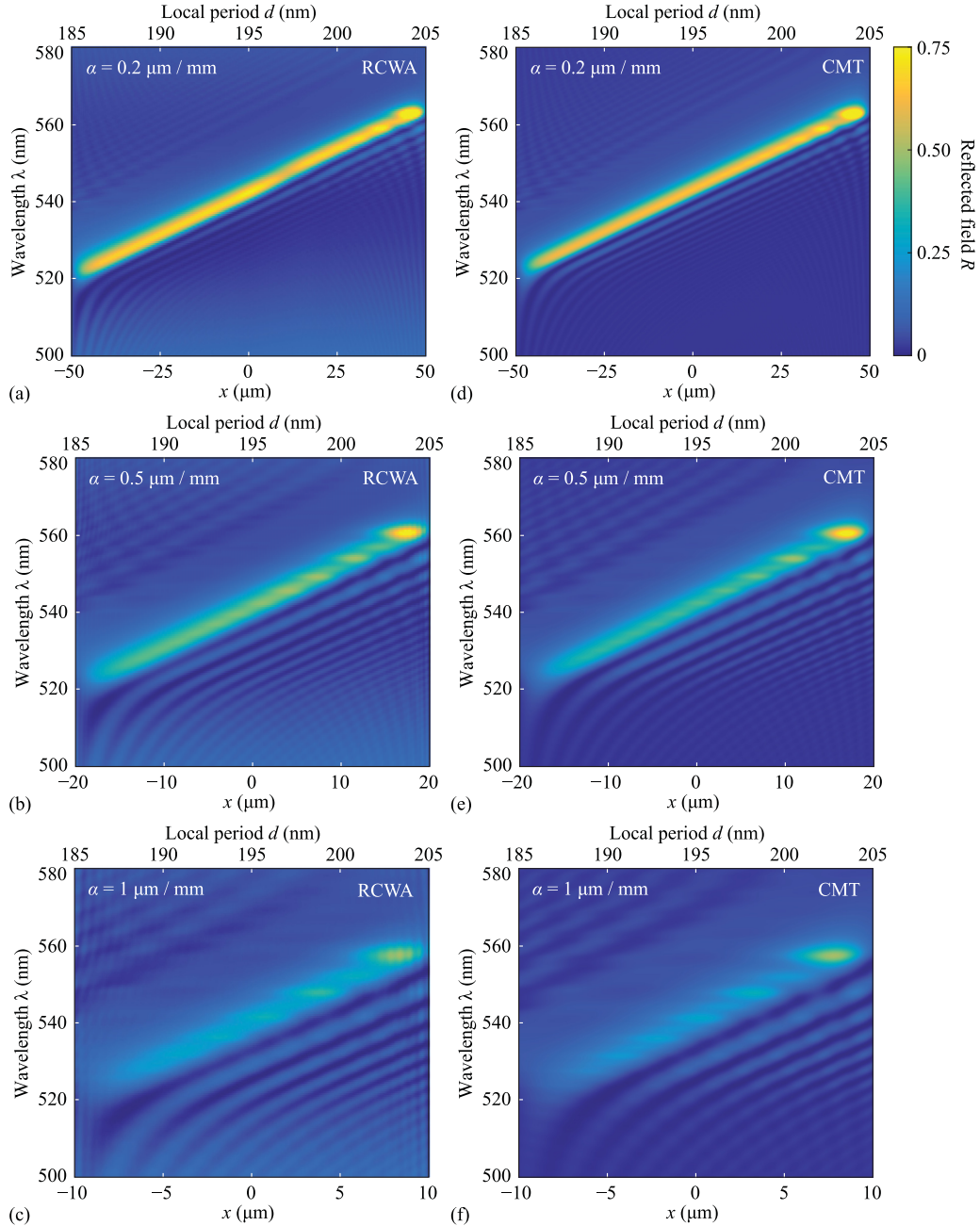
FIG. 3. Reflected field distributions R calculated at different wavelengths of the incident plane wave and different positions along the structure using (a)–(c) RCWA ($R = |E_y|^2$) and (d)–(f) using CMT ($R = |f_R|^2$). The subplots correspond to different period change rates: (a) and (d) $\alpha = 0.2\ \mu$m/mm, (b) and (e) $\alpha = 0.5\ \mu$m/mm, and (c) and (f) $\alpha = 1\ \mu$m/mm. The presented color map applies to all subplots.

normalized cross sections at $x = 0$ (local period $d = 195$nm) are presented in Fig. 4. From Fig. 4, it can be clearly seen that with an increase in α, the FWHM of the resonances increases and amounts to 2.5, 4.7, 7.9, and 10.3 nm for $\alpha = 0, 0.2, 0.5$, and 1 μm/mm, respectively. In addition, the line shape of the resonance depends significantly on the period change rate α: at $\alpha = 0$, the resonance has a Fano line shape, which is close to the symmetric Lorentzian line shape for the considered structure; at greater α values, the broadening of the resonant peak is accompanied by a change in shape and the appearance of secondary maxima at shorter wavelengths. We will explain

the appearance of these secondary maxima, which become more pronounced at greater α values, in the following section.

IV. LOCAL PHOTONIC BAND STRUCTURE

Let us consider the reflected field distribution along the varying-period structure at the wavelength $\lambda = 544$ nm [Fig. 5(a)]. This distribution was calculated for $\alpha = 0.5\ \mu$m/mm and therefore is a horizontal cross section of Fig. 3(b). Like in Fig. 4, the field distribution is essentially asymmetric with secondary maxima present to the right of
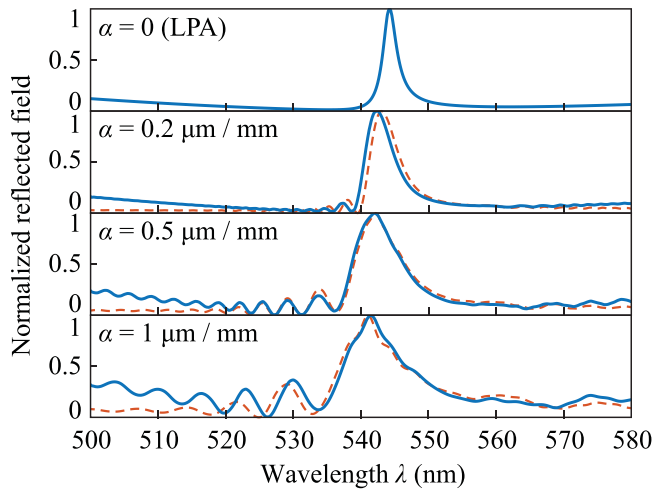
FIG. 4. Normalized spectra of the field reflected by the structure at $x = 0$ at different period change rates α: RCWA simulations (solid blue lines) and CMT predictions (dashed red lines). The first plot ($\alpha = 0$) was calculated using the local periodic approximation.

the main peak. To explain this fact, let us consider the local dispersion of the eigenmodes of the investigated structure.

Figure 5(b) shows the rigorously calculated [47,48] dispersion of the TE-polarized eigenmodes of strictly periodic gratings with the periods d equal to 190, 195, and 200 nm.
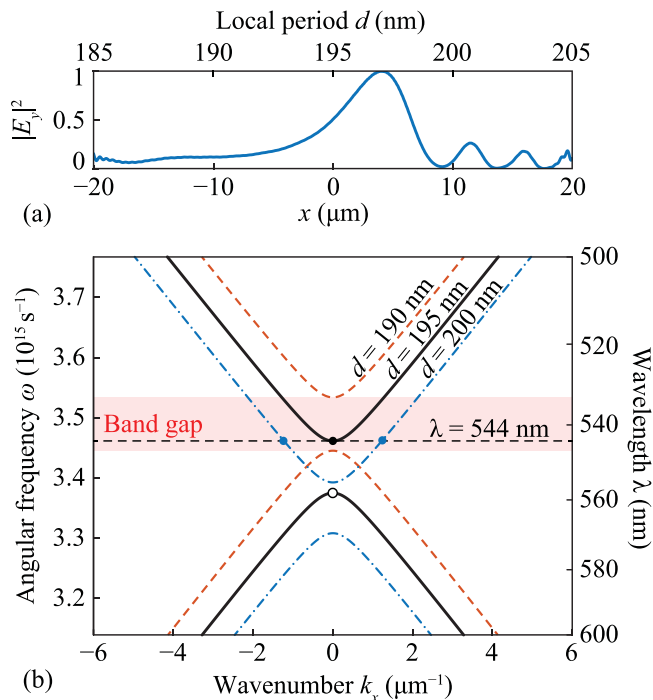

FIG. 5. (a) Normalized reflected field distribution along the varying-period structure at the wavelength $\lambda = 544$ nm for $\alpha = 0.5$ μm/mm. (b) Local band diagram at different local periods: $d = 190$ nm (dashed red curves), $d = 195$ nm (solid black curves), and $d = 200$ nm (dash-dotted blue curves). Horizontal dashed line shows the wavelength of $\lambda = 544$ nm. The band gap at $d = 190$ nm is shown in red.

According to Fig. 5(b), at $d = 195$ nm, the eigenmode is excited at normal incidence at $\lambda = 544$ nm. This eigenmode is the even (symmetric) one and is marked with a solid black dot on the upper solid black curve, whereas the odd (antisymmetric) mode is marked with a black circle on the lower solid black curve. The frequency range lying between these two modes constitutes the band gap of the structure, where no modes can propagate in the $\pm x$ directions. With an increase in the grating period, the dispersion curves (and, consequently, the band gap) will "move down" to the longer wavelengths (see the dash-dotted blue curves). Decreasing the period will shift the dispersion curves "up" to the shorter wavelengths (see the dashed red curves).

Let us now discuss how the local dispersion law determines the optical properties of the varying-period structure and, in particular, the reflected field distribution. To do this, we consider the normal incidence of a monochromatic TE-polarized plane wave. At a certain local period, the in-plane wave-vector components of the positive and negative first diffraction orders will match the wave number (propagation constant) of the eigenmode supported by the waveguide layer at the incident wavelength. For the considered example ($\lambda = 544$ nm), this happens at the points of the structure where the local period is close to 195 nm. In this region, the incident energy is efficiently coupled to the waveguide layer, and the excited modes propagate to the left and to the right inside the waveguide.

When the light propagates to the left, the local period decreases, and the incident wavelength enters the band gap of the "local" grating [see Fig. 5(b)]. In the band gap, there are no modes that can carry energy, and the mode becomes reflected to the right instead of propagating to the left. In contrast, when the light propagates to the right, two counterpropagating eigenmodes [blue dots in Fig. 5(b)] that can carry energy at the considered wavelength appear. Upon propagation, these eigenmodes leak out of the waveguide with the leakage direction varying along the structure, which gives the secondary peaks discussed above.

The presented local photonic band structure analysis gives a rough qualitative explanation of the asymmetric field distribution in the considered structure. Let us note that the plots in Fig. 3 are almost translationally invariant along an inclined straight line in the λ-x parameter space. Therefore, the vertical and horizontal cross sections of each plot have approximately the same shape, and hence, the presented local photonic band description also explains the asymmetric line shape of the resonance with respect to the varying wavelength (see Fig. 4). A more accurate, quantitative description can be obtained using the coupled-mode theory derived in the next section.

V. COUPLED-MODE THEORY

In this section, we develop a spatiotemporal coupled-mode theory describing the optical properties of a varying-period guided-mode resonant grating. First, we revisit the CMT for the case of a strictly periodic grating, and then we introduce spatial variation of the parameters of the model to take into account the period change rate α and apply the obtained theory to the considered grating example.

A. Periodic grating

To describe the optical properties of a symmetric grating with a fixed period d_0, let us write the coupled-mode theory in the form of two coupled unidirectional wave equations [49]:

$$
\begin{aligned}
\frac{\partial u}{\partial t} &= -v_{\mathrm{g}}\frac{\partial u}{\partial x} + i(k_{\mathrm{mode}}v_{\mathrm{g}} - \omega_0)u \\
&\quad - \gamma u + \kappa e^{2ik_{x,\mathrm{gr}}x}v + qf(x,t)e^{ik_{x,\mathrm{gr}}x}, \\
\frac{\partial v}{\partial t} &= v_{\mathrm{g}}\frac{\partial v}{\partial x} + i(k_{\mathrm{mode}}v_{\mathrm{g}} - \omega_0)v \\
&\quad - \gamma v + \kappa e^{-2ik_{x,\mathrm{gr}}x}u + qf(x,t)e^{-ik_{x,\mathrm{gr}}x}.
\end{aligned}
\tag{4}
$$

Here, u and v denote the complex amplitudes of the modes propagating inside the waveguide in the positive and negative directions of the x axis, respectively. The dispersion of these modes is assumed to be linear near the frequency ω_0 and is defined by the group velocity v_{g} and the wave number k_{mode} at this frequency.

The coupling coefficients γ, κ, and q describe the following scattering processes: mode leakage is described by the real leakage rate γ; coupling between modes u and v is described by the complex coefficient κ, and mode excitation by the incident field $f(x,t)$ is described by the complex coupling coefficient q. The coupling and excitation of the modes occur due to the diffraction of light into one of the diffraction orders. Assuming that the modes are excited by the positive and negative first diffraction orders (which is the case for the structures considered throughout this work), the corresponding phase change is described by the exponents [49,50] in Eq. (4) with

$$
k_{x,\mathrm{gr}} = \frac{2\pi}{d_0}.
\tag{5}
$$

The eigenmodes are excited by a normally incident plane wave with frequency ω_0 when the wave number of the mode at this frequency coincides with the in-plane wave-vector component of the first diffraction order: $k_{x,\mathrm{gr}} = k_{\mathrm{mode}}$.

Note that for a symmetric lossless grating, the coefficients ω_0, γ, and κ can be expressed in terms of complex frequencies of the eigenmodes of the grating at the center of the first Brillouin zone in the following form [49]:

$$
\begin{aligned}
\omega_0 &= \mathrm{Re}\,\frac{\omega_{\mathrm{p1}} + \omega_{\mathrm{p2}}}{2}, \\
\gamma &= -\mathrm{Im}\,\frac{\omega_{\mathrm{p1}} + \omega_{\mathrm{p2}}}{2}, \\
\kappa &= \frac{\omega_{\mathrm{p1}} - \omega_{\mathrm{p2}}}{2i}.
\end{aligned}
\tag{6}
$$

Here, ω_{p1} and ω_{p2} are the complex frequencies of the symmetric (even) and antisymmetric (odd) eigenmodes, which are shown in Fig. 5(b) with a solid black dot and a black circle, respectively.

The complex amplitude of the reflected field can be written as [49]

$$
f_R(x,t) = r_0 f(x,t) + q_r u(x,t)e^{-ik_{x,\mathrm{gr}}x} + q_r v(x,t)e^{ik_{x,\mathrm{gr}}x},
\tag{7}
$$

where the first term describes the nonresonant scattering and the other terms contain the resonant contribution due to the

energy leakage from modes u and v. Thus, the coefficient r_0 can be referred to as the nonresonant reflection coefficient, and q_r is the "mode-to-superstrate" leakage rate. A similar equation, which is not presented here for the sake of brevity, can be written for the transmitted field.

In the presented coupled-mode equations, we considered a periodic structure with the symmetry plane $x = 0$. For further analysis, we will also be interested in considering a symmetric grating that is shifted by a distance Δ along the x axis. The coupled-mode equations for such a structure can be obtained by replacing x with $x + \Delta$ in the exponents of Eqs. (4) and (7).

It is worth mentioning that applying the two-dimensional Fourier transform to Eqs. (4) and (7) with respect to t and x allows one to obtain the reflection coefficient of a strictly periodic grating as a function of the angular frequency ω and the in-plane wave-vector component k_x of the incident wave [see Eq. (A1) in the Appendix] [49].

B. Grating with a linearly varying period

As we discussed in Sec. II, the permittivity of the varying-period structure is given by $\varepsilon(x/D(x))$. Let us consider the permittivity in the vicinity of the point $x = x_0$ and replace the argument of the function ε with the first two terms of its Taylor series:

$$
\varepsilon\left(\frac{x}{D(x)}\right) \approx \varepsilon\left(\frac{x - \Delta(x_0)}{d(x_0)}\right),
$$

where $\Delta(x_0) = x_0[1 - d(x_0)/D(x_0)]$, which follows from Eq. (2). The obtained equation means that we can locally approximate the varying-period structure with the fixed-period one having the period equal to the local period $d(x_0)$ and shifted by $\Delta(x_0)$. On the other hand, by replacing x with $x + \Delta$ in Eqs. (4) and (7), we can see that we can take into account the offset Δ by using Eqs. (4) and (7) with $k_{x,\mathrm{gr}}$ redefined as

$$
k_{x,\mathrm{gr}}(x) = \frac{2\pi}{D(x)}.
\tag{8}
$$

This means that local approximation of the varying-period grating at the point $x = x_0$ with a grating with the fixed period $d(x_0)$ that is shifted by $\Delta(x_0)$ is formally equivalent to approximating it with a nonshifted grating with the fixed period $D(x_0)$.

Let us note that in the "conventional" LPA (see Fig. 2), the strictly periodic grating locally approximating the varying-period structure is used to calculate the local reflectance. In contrast, in the approach discussed in this section, we locally approximate a varying-period structure with strictly periodic ones to derive the CMT with spatially varying parameters. As we will show below, this approach is much more accurate and enables describing the influence of the period change rate on the resonance line shape. It is also worth mentioning that in the case of a varying-period structure, all the other parameters (k_{mode}, v_{g}, ω_0, γ, κ, q, q_r, r_0) in the coupled-mode equations (4) and (7) also become functions of the spatial coordinate x. However, in what follows, we will take into account only the dependence of $k_{x,\mathrm{gr}}$ on x [Eq. (8)], which, as it turns out, has the highest impact on the optical properties

of the varying-period grating, whereas the other parameters can be assumed to be constant. As a result, the x dependence will appear only under the exponents in Eq. (4).

To write the CMT for a varying-period structure, let us assume that the incident light is a monochromatic plane wave with unit amplitude, which normally impinges on the grating: $f(x, t) = e^{-i\omega t}$. In this case, the mode amplitudes u and v will also depend on time as $e^{-i\omega t}$. Therefore, we can rewrite the system of Eqs. (4) and (7) in terms of the functions $\tilde{u}(x) = u(x, t) e^{-ik_{x,\text{gr}}(x)x} e^{i\omega t}$ and $\tilde{v}(x) = v(x, t) e^{ik_{x,\text{gr}}(x)x} e^{i\omega t}$ depending solely on the spatial coordinate x:

$$-i\omega\tilde{u} = v_{\text{g}}\left[-\frac{d\tilde{u}}{dx} - i\tilde{u}\frac{d[x k_{x,\text{gr}}(x)]}{dx} + ik_{x,\text{gr}}(0)\tilde{u}\right]$$
$$-i\omega_0\tilde{u} - \gamma\tilde{u} + \tilde{v} + q,$$

$$-i\omega\tilde{v} = v_{\text{g}}\left[\frac{d\tilde{v}}{dx} - i\tilde{v}\frac{d[x k_{x,\text{gr}}(x)]}{dx} + ik_{x,\text{gr}}(0)\tilde{v}\right]$$
$$-i\omega_0\tilde{v} - \gamma\tilde{v} + \kappa\tilde{u} + q,$$

$$\tilde{f}_R(x, \omega) = r_0 + q_r\tilde{u} + q_r\tilde{v}. \tag{9}$$

Here, $\tilde{f}_R = f_R e^{i\omega t}$ is the reflected field at the position x of the varying-period grating calculated at the angular frequency of the incident light ω. Note that in Eq. (9), we assumed $k_{\text{mode}} = k_{x,\text{gr}}(0)$. By doing this, we required that at the angular frequency ω_0, the wave number of the mode should match the wave number of the first diffraction order at $x = 0$; therefore, the eigenmode is excited at this point at the specified frequency [see the discussion after Eq. (5)].

From Eqs. (2) and (8), it follows that $d[x k_{x,\text{gr}}(x)]/dx = 2\pi/d(x)$ and $k_{x,\text{gr}}(0) = 2\pi/d(0)$. Therefore, we can rewrite Eq. (9) as

$$v_{\text{g}}\frac{d\tilde{u}}{dx} = \left[i(\omega - \omega_0) - \gamma + 2\pi iv_{\text{g}}\left(\frac{1}{d(0)} - \frac{1}{d(x)}\right)\right]\tilde{u}$$
$$+ \kappa\tilde{v} + q,$$

$$-v_{\text{g}}\frac{d\tilde{v}}{dx} = \left[i(\omega - \omega_0) - \gamma + 2\pi iv_{\text{g}}\left(\frac{1}{d(0)} - \frac{1}{d(x)}\right)\right]\tilde{v}$$
$$+ \kappa\tilde{u} + q,$$

$$\tilde{f}_R(x, \omega) = r_0 + q_r\tilde{u} + q_r\tilde{v}. \tag{10}$$

The obtained system of equations (10) constitutes the coupled-mode theory for the considered varying-period guided-mode resonant gratings. It is important to note that it is valid for any (not necessarily linear) local period variation law $d(x)$.

Now, let us assume that the local period varies linearly [Eq. (1)] and the period change rate α is small enough to enable replacing $1/d(x)$ with only the first two terms of its Taylor series with respect to α:

$$\frac{1}{d(x)} = \frac{1}{d_0 + \alpha x} \approx \frac{1}{d_0} - \frac{\alpha}{d_0^2}x + O(\alpha^2).$$

This brings us to the following linearized coupled-mode equations:

$$v_{\text{g}}\frac{d\tilde{u}}{dx} = \left[i(\omega - \omega_0) - \gamma + i\alpha\frac{2\pi v_{\text{g}}}{d_0^2}x\right]\tilde{u} + \kappa\tilde{v} + q,$$

$$-v_{\text{g}}\frac{d\tilde{v}}{dx} = \left[i(\omega - \omega_0) - \gamma + i\alpha\frac{2\pi v_{\text{g}}}{d_0^2}x\right]\tilde{v} + \kappa\tilde{u} + q,$$

$$\tilde{f}_R(x, \omega) = r_0 + q_r\tilde{u} + q_r\tilde{v}. \tag{11}$$

From these equations, it follows that

$$\tilde{f}_R(x + \delta, \omega) = \tilde{f}_R\left(x, \omega + \alpha\delta\frac{2\pi v_{\text{g}}}{d_0^2}\right),$$

which means that a change δ in the position x along the structure is equivalent to a frequency shift $\alpha\delta 2\pi v_{\text{g}}/d_0^2$, which agrees with the analysis based on the empty-lattice approximation. Since α is assumed to be small, the equivalent shift in wavelength is $-\alpha\delta(\lambda/d_0)^2 v_{\text{g}}/c$, which explains the approximate translational invariance of the plots in Fig. 3 that was used when discussing the local photonic band structure in Sec. IV.

C. Simulation results

In order to verify the developed CMT, we numerically solved the system (10) for the varying-period gratings considered in Secs. II and III. Note that we used the more accurate system (10) [however, system (11) gives very similar results]. In the calculations, we used the following values of the parameters of the model:

$$\omega_{\text{p1}} = 3.4616 \times 10^{15} - 7.8216 \times 10^{12} i\,\text{s}^{-1},$$
$$\omega_{\text{p2}} = 3.3752 \times 10^{15}\,\text{s}^{-1},$$
$$v_{\text{g}} = 0.27953c,$$
$$qq_r = (2.7910 + 2.0017i) \times 10^{12}\,\text{s}^{-1},$$
$$r_0 = 0.15012 - 0.013279i.$$

Note that the values ω_{p1} and ω_{p2} determine ω_0, γ, and κ through Eq. (6). It is also important to note that, as discussed above in Sec. V B, all the presented parameters were calculated by considering only the strictly periodic grating (in the studied example, the grating with the period $d_0 = 195$ nm). A detailed description of the parameter calculation process is presented in the Appendix.

In order to solve Eqs. (10) numerically, one needs to impose boundary conditions. We used the conditions

$$u(-W/2) = 0,$$
$$v(W/2) = 0, \tag{12}$$

which are similar to the PML conditions used in the RCWA simulations presented in Sec. III. Indeed, according to Eqs. (12), there is no mode propagating to the right at the left boundary (at $x = -W/2$). Therefore, the v mode propagating to the left is not reflected at this boundary. Similarly, the right boundary ($x = W/2$) does not "emit" modes propagating to the left.

The reflected field distributions calculated using the developed CMT of Eq. (10) with the boundary conditions (12) are
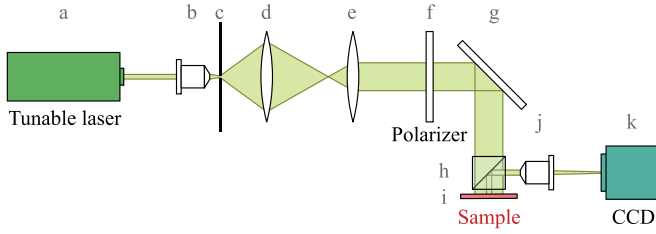
FIG. 6. Optical setup: (a) light source, (b) 20× micro-objective, (c) 40-μm pinhole, (d) and (e) lenses, (f) polarizer, (g) mirror, (h) beam-splitting cube, (i) sample varying-period grating, (j) 10× micro-objective, and (k) CCD matrix.

presented in Figs. 3(d)–3(f). It is evident from Fig. 3 that the CMT predictions (right column) are in excellent agreement with the rigorous simulation results based on RCWA (left column). For the sake of comparison, we also presented the CMT predictions calculated at a fixed point ($x = 0$) in Fig. 4 (dashed red lines). We believe that the slight differences between the RCWA and CMT results are mainly due to the fact that in the CMT calculations, we assumed that the nonresonant reflection coefficient r_0 does not depend on frequency. Let us also note that the fact that we replaced part of the varying period grating with PMLs in the RCWA simulations [or used equivalent boundary conditions of Eq. (12) in the CMT] means that the modes that would have been excited by these parts of the grating do not contribute to the field distributions shown in Fig. 3. This results in "bending" of the secondary maxima, which is clearly seen in Fig. 3 in the wavelength range $\lambda \in [500, 520]$ nm and local period range $d \in [185, 190]$ nm for the distributions calculated using both RCWA and the proposed CMT.

VI. EXPERIMENT

In this section, we present the results of a proof-of-concept experiment confirming the validity of the developed theoretical model. In this regard, it is important to note that the presented coupled-mode theory can be applied not only to the varying-period guided-mode resonant filters considered above exhibiting a well-defined "main" resonant reflectance peak on a low background but also to other varying-period guided-mode resonant gratings. For the experimental investigation, we fabricated such varying-period gratings patterned in a polymethylmethacrylate (PMMA) layer using a XENOS XeDraw 2 *e*-beam lithography device with a Carl Zeiss Supra 25 electron microscope. The PMMA layer was spin coated on top of a TiO$_2$ waveguide layer sputtered on a fused-silica substrate. The thicknesses and the refractive indices of the deposited layers were controlled using a spectroscopic ellipsometer Woollam M-2000. The fabricated structures have the following parameters: grating thickness $h_{gr} = 300$ nm, waveguide layer thickness $h_{wg} = 130$ nm, grating fill factor $f = 1/2$, and grating central period $d_0 = 330$ nm. Three varying-period samples were fabricated, each having the same dimensions (100×100 μm^2) but different period change rates α: 0.25, 0.5, and 1 μm/mm.

The optical setup utilized for the experimental investigation of the fabricated gratings is shown in Fig. 6. As a

light source (labeled a), we used a tunable laser EKSPLA NT242. To generate a collimated optical beam, we used a 20× micro-objective (labeled b), a pinhole with 40-μm aperture (labeled c) acting as a secondary point light source, and a collimator consisting of a pair of lenses (labeled d and e). The required TE polarization of the generated beam was set using a polarizer (labeled f). After being reflected by a mirror (labeled g) and passing through a beam-splitting cube (labeled h) used to separate the incident and reflected light (Fig. 6), the beam impinged on the investigated varying-period grating (labeled i). The radiation reflected from the grating was imaged on a CCD matrix (labeled k) using a 10× micro-objective (labeled j).

The measured reflected field distributions at $\lambda = 626$ nm for the three fabricated gratings are shown in Figs. 7(a)–7(c). Figures 7(d)–7(f) show the corresponding field cross sections averaged along the vertical direction for wavelengths of 618, 626, and 633 nm. Figures 7(g)–7(i) show the model field distributions calculated using the proposed coupled-mode equations (10) with the following parameters:

$$\omega_{p1} = 3.0530 \times 10^{15} - 2.7806 \times 10^{12} i \, \text{s}^{-1},$$
$$\omega_{p2} = 3.0510 \times 10^{15} \, \text{s}^{-1},$$
$$v_g = 0.37296c,$$
$$qq_r = (-1.1848 + 0.55954i) \times 10^{12} \, \text{s}^{-1},$$
$$r_0 = 0.13732 - 0.012337i. \tag{13}$$

It is evident from Figs. 7(d)–7(i) that the predictions of the coupled-mode theory are in good agreement with the experimental results.

Let us note that compared to the structure investigated in Secs. II–V, the fabricated structure has higher group velocity v_g of the modes. As a result, the secondary peaks are more pronounced and are comparable in magnitude to the main ("central") peak. Moreover, according to Eq. (13), the band gap of the fabricated structure is very narrow (the difference between the wavelengths of the even and odd modes is less than 1 nm). Such a narrow band gap allows the modes to tunnel through, which results in the appearance of secondary peaks both to the left and to the right of the central peak. Nevertheless, all these features are well reproduced by the developed CMT.

VII. CONCLUSION

In the present work, we investigated optical properties of guided-mode resonant gratings with linearly varying period. We considered period variation rates up to 1 μm/mm, which significantly exceeds the values considered in the majority of previously published works, and, using full-wave numerical simulations based on the rigorous coupled-wave analysis, demonstrated that in this case, the local periodic approximation usually used for describing the optical properties of such structures becomes inapplicable. We qualitatively explained the asymmetric non-Fano resonance shapes with secondary maxima appearing at high period change rates by examining the local band structure of the varying-period gratings. In order to obtain an accurate quantitative description, we developed a spatiotemporal coupled-mode theory for gratings
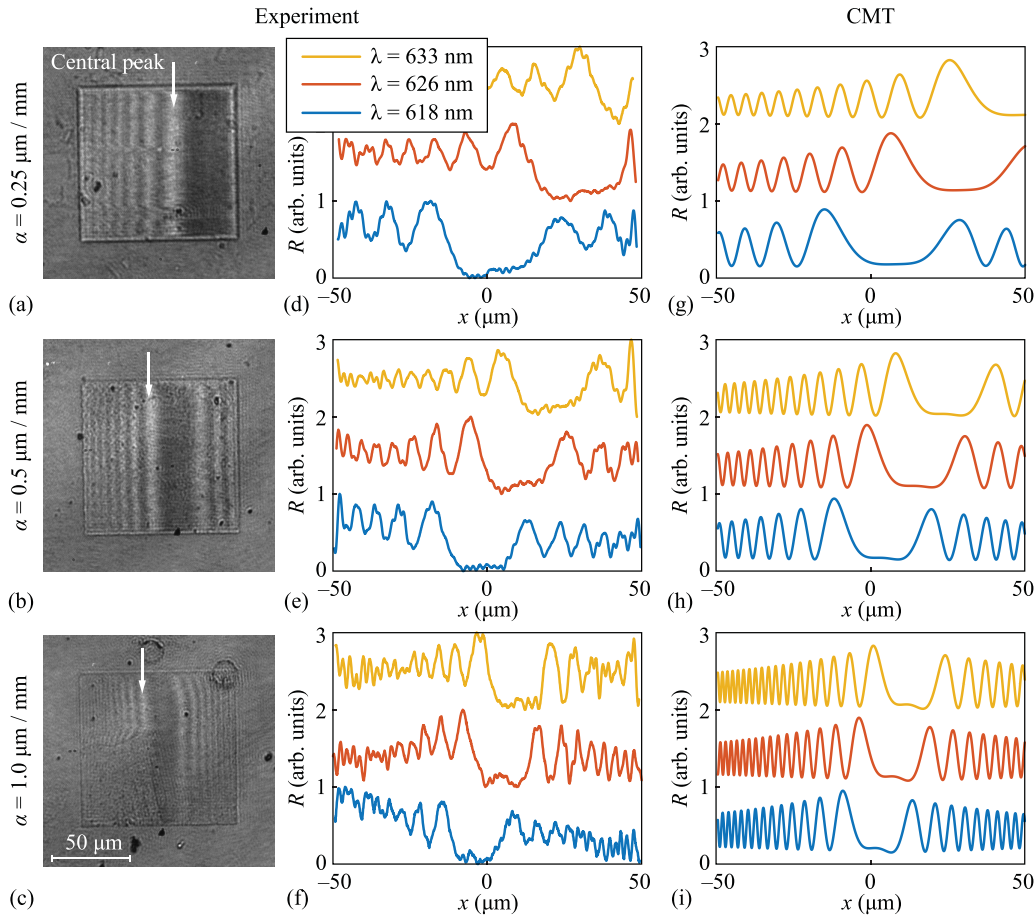
FIG. 7. (a)–(c) Experimentally obtained reflected field distributions at $\lambda = 626$ nm and (d)–(f) normalized averaged cross sections of such distributions at wavelengths $\lambda = 633$ nm (yellow upper lines), $\lambda = 626$ nm (red middle lines), and $\lambda = 618$nm (blue lower lines). The lines for $\lambda = 626$ nm and $\lambda = 633$ nm are vertically offset by 1 and 2, respectively, for the sake of visual clarity. (g)–(i) Reflected field distributions predicted by the coupled-mode theory at the same wavelengths. Field distributions are presented for three different period change rates: (a), (d), and (g) $\alpha = 0.25$ μm/mm, (b), (e), and (h) $\alpha = 0.5$ μm/mm, and (c), (f), and (i) $\alpha = 1$ μm/mm.

with a spatially varying period. The developed model does not require fitting of any parameters since their values are determined by analyzing a strictly periodic guided-mode resonant grating. At all the considered period change rates, the predictions of the derived CMT model are in good agreement with the numerical simulation results and with the results of a proof-of-concept experiment, which included the fabrication of resonant varying-period gratings and the investigation of their optical properties.

We believe that the presented results are important for the design of compact linear variable filters based on varying-period guided-mode resonant gratings. In particular, the presented coupled-mode theory can be used for estimating the achievable spectral resolution of such filters. In this regard, it is important to mention that the calculation of the reflection spectra using the derived CMT model is several orders of magnitude faster than the full-wave electromagnetic simulation. In particular, the computation of the data for Fig. 3(a) using RCWA took about 3 h, whereas the CMT-based calculations [Fig. 3(d)] required less than a minute. At the same time, it is evident that the model "captures" the main effects occurring in the varying-period structures such as the appearance of secondary maxima of the reflected field, their magnitude,

and the spacing between them along the periodicity direction.

An analytical or semianalytical investigation of the equations of the derived CMT model may lead to approximate closed-form estimates of the linewidth and the line shape of the resonances. In our opinion, the presented results can also be extended to other resonant (quasi)periodic structures with spatially varying parameters, e. g., guided-mode gratings with varying thickness of the waveguide layer or photonic crystal slabs with varying height, as well as structures with several simultaneously varying parameters. This will be the subject of future research.

APPENDIX: CALCULATING THE PARAMETERS OF THE COUPLED-MODE THEORY

In this Appendix, we describe the calculation of the parameters used in the spatiotemporal coupled-mode theory. This

theory gives the following approximate expression for the reflection coefficient of a fixed-period guided-mode resonant grating [49]:

$$r(\omega, k_x) = r_0 \frac{v_g^2 k_x^2 - (\omega - \omega_z)(\omega - \omega_{p2})}{v_g^2 k_x^2 - (\omega - \omega_{p1})(\omega - \omega_{p2})}, \quad (A1)$$

where

$$\omega_z = \omega_{p1} - 2iqq_r/r_0. \quad (A2)$$

Taking into account Eqs. (6) and (A2), one can see that Eq. (A1) contains all the parameters used in Eq. (10), which is the main equation of this work describing varying-period resonant gratings. Therefore, these parameters can be estimated by requiring that Eq. (A1) approximate well the rigorously calculated reflection spectrum $r_{RCWA}(\omega, k_x)$ of a fixed-period grating. However, finding these parameters by simply fitting Eq. (A1) to the rigorously calculated spectrum gives, as a rule, poor results. Below, we present another approach based on the calculation of the eigenmodes of the structure, which is fast and robust.

First, we assume $k_x = 0$. According to Eq. (A1), in this case, the scattering matrix $\mathbf{S}(\omega, k_x = 0)$ of the structure has two complex poles ω_{p1} and ω_{p2}, which are the frequencies of the eigenmodes of the structure. These poles can be rigorously calculated using the numerical approach presented in [48].

Then, we pick a real frequency near these eigenfrequencies [e.g., the frequency $\omega_0 = \text{Re}(\omega_{p1} + \omega_{p2})/2$]. In this case, the scattering matrix $\mathbf{S}(\omega = \omega_0, k_x)$ considered as a function of k_x has two poles $k_x = \pm k_p$, which describe the complex-wave-number eigenmodes of the structure. As above, we calculate

the value of k_p using the numerical approach of [48]. By equating the denominator in Eq. (A1) at $\omega = \omega_0$, $k_x = k_p$ to zero, we obtain the group velocity as

$$v_g = \text{Re} \frac{\sqrt{(\omega_0 - \omega_{p1})(\omega_0 - \omega_{p2})}}{k_p}.$$

Note that the group velocity in the CMT is real, so taking the real part here is to eliminate numerical errors resulting in a small imaginary part.

Then, we calculate the parameter ω_z, which, according to Eq. (A1), is the angular frequency value providing a reflection zero in the case of normal incidence. Hence, ω_z can be found by numerically solving the equation $r_{RCWA}(\omega_z, 0) = 0$.

Next, to find the nonresonant reflection coefficient r_0, we equate the rigorously calculated reflection coefficient and the CMT prediction of Eq. (A1) in the case of normal incidence ($k_x = 0$) at the frequency ω_0: $r(\omega_0, 0) = r_{RCWA}(\omega_0, 0)$. This gives us

$$r_0 = r_{RCWA}(\omega_0, 0) \frac{\omega_0 - \omega_z}{\omega_0 - \omega_{p2}}.$$

Finally, the product qq_r can be expressed from Eq. (A2) as

$$qq_r = ir_0 \frac{\omega_z - \omega_{p1}}{2}.$$

To summarize, the presented approach is based on finding the values ω_{p1}, ω_{p2}, k_p, and ω_z. The calculation of each of these parameters requires a numerical solution of an equation involving the RCWA-calculated scattering matrix of a fixed-period grating. One more scattering matrix calculation is required for estimating the nonresonant reflection coefficient r_0. For the structures considered in this work, these computations take less than 2 s.

[1] W. Zhou, D. Zhao, Y.-C. Shuai, H. Yang, S. Chuwongin, A. Chadha, J.-H. Seo, K. X. Wang, V. Liu, Z. Ma, and S. Fan, Progress in 2D photonic crystal Fano resonance photonics, Prog. Quantum Electron. **38**, 1 (2014).

[2] A. E. Miroshnichenko, S. Flach, and Y. S. Kivshar, Fano resonances in nanoscale structures, Rev. Mod. Phys. **82**, 2257 (2010).

[3] R. W. Wood, XLII. On a remarkable case of uneven distribution of light in a diffraction grating spectrum, London, Edinburgh Dublin Philos. Mag. J. Sci. **4**, 396 (1902).

[4] Lord Rayleigh, On the dynamical theory of gratings, Proc. R. Soc. London, Ser. A **79**, 399 (1907).

[5] U. Fano, The theory of anomalous diffraction gratings and of quasi-stationary waves on metallic surfaces (Sommerfeld's waves), J. Opt. Soc. Am. **31**, 213 (1941).

[6] A. Hessel and A. A. Oliner, A new theory of Wood's anomalies on optical gratings, Appl. Opt. **4**, 1275 (1965).

[7] S. Collin, Nanostructure arrays in free-space: Optical properties and applications, Rep. Prog. Phys. **77**, 126402 (2014).

[8] P. Qiao, W. Yang, and C. J. Chang-Hasnain, Recent advances in high-contrast metastructures, metasurfaces, and photonic crystals, Adv. Opt. Photonics **10**, 180 (2018).

[9] G. Quaranta, G. Basset, O. J. Martin, and B. Gallinet, Recent advances in resonant waveguide gratings, Laser Photonics Rev. **12**, 1800017 (2018).

[10] S. S. Wang, R. Magnusson, J. S. Bagby, and M. G. Moharam, Guided-mode resonances in planar dielectric-layer diffraction gratings, J. Opt. Soc. Am. A **7**, 1470 (1990).

[11] S. S. Wang and R. Magnusson, Theory and applications of guided-mode resonance filters, Appl. Opt. **32**, 2606 (1993).

[12] R. Magnusson and S. S. Wang, New principle for optical filters, Appl. Phys. Lett. **61**, 1022 (1992).

[13] S. Tibuleac and R. Magnusson, Reflection and transmission guided-mode resonance filters, J. Opt. Soc. Am. A **14**, 1617 (1997).

[14] Z. S. Liu, S. Tibuleac, D. Shin, P. P. Young, and R. Magnusson, High-efficiency guided-mode resonance filter, Opt. Lett. **23**, 1556 (1998).

[15] A. Emadi, H. Wu, G. de Graaf, and R. Wolffenbuttel, Design and implementation of a sub-nm resolution microspectrometer based on a linear-variable optical filter, Opt. Express **20**, 489 (2012).

[16] N. P. Ayerden, G. de Graaf, and R. F. Wolffenbuttel, Compact gas cell integrated with a linear variable optical filter, Opt. Express **24**, 2981 (2016).

[17] A. Emadi, H. Wu, G. de Graaf, P. Enoksson, J. H. Correia, and R. Wolffenbuttel, Linear variable optical filter-based ultraviolet microspectrometer, Appl. Opt. **51**, 4308 (2012).

[18] K. Hendrix, Linear variable filters for NASA's OVIRS instrument: Pushing the envelope of blocking, Appl. Opt. **56**, C201 (2017).

[19] B. Sheng, P. Chen, C. Tao, R. Hong, Y. Huang, and D. Zhang, Linear variable filters fabricated by ion beam etching with triangle-shaped mask and normal film coating technique, Chin. Opt. Lett. **13**, 122301 (2015).

[20] L. Qian, D. Zhang, C. Tao, R. Hong, and S. Zhuang, Tunable guided-mode resonant filter with wedged waveguide layer fabricated by masked ion beam etching, Opt. Lett. **41**, 982 (2016).

[21] L. Qian, K. Wang, and C. Han, Tunable filter with varied-line-spacing grating fabricated using holographic recording, IEEE Photonics Technol. Lett. **29**, 925 (2017).

[22] D. W. Dobbs, I. Gershkovich, and B. T. Cunningham, Fabrication of a graded-wavelength guided-mode resonance filter photonic crystal, Appl. Phys. Lett. **89**, 123113 (2006).

[23] N. Ganesh, A. Xiang, N. B. Beltran, D. W. Dobbs, and B. T. Cunningham, Compact wavelength detection system incorporating a guided-mode resonance filter, Appl. Phys. Lett. **90**, 081103 (2007).

[24] H.-Y. Hsu, Y.-H. Lan, and C.-S. Huang, A gradient grating period guided-mode resonance spectrometer, IEEE Photonics J. **10**, 4500109 (2018).

[25] L. Liu, H. A. Khan, J. Li, A. C. Hillier, and M. Lu, A strain-tunable nanoimprint lithography for linear variable photonic crystal filters, Nanotechnology **27**, 295301 (2016).

[26] B. Sheng, L. Luo, Y. Huang, G. Chen, H. Zhou, D. Zhang, and S. Zhuang, Tailorable elastomeric grating with tunable groove density gradient, IEEE Photonics J. **9**, 2400406 (2017).

[27] Y.-C. Wang, W-Y. Jang, and C.-S. Huang, Lightweight torque sensor based on a gradient grating period guided-mode resonance filter, IEEE Sens. J. **19**, 6610 (2019).

[28] H.-A. Lin, H.-Y. Hsu, C.-W. Chang, and C.-S. Huang, Compact spectrometer system based on a gradient grating period guided-mode resonance filter, Opt. Express **24**, 10972 (2016).

[29] C.-T. Hsiung and C.-S. Huang, Refractive index sensor based on a gradient grating period guided-mode resonance, IEEE Photonics Technol. Lett. **31**, 253 (2019).

[30] C.-W. Chang, S.-T. Chen, Y.-M. Lin, and C.-S. Huang, Resonant wavelength shift detection system based on a gradient grating period guided-mode resonance, IEEE Photonics J. **10**, 6803010 (2018).

[31] H.-A. Lin and C.-S. Huang, Linear variable filter based on a gradient grating period guided-mode resonance filter, IEEE Photonics Technol. Lett. **28**, 1042 (2016).

[32] F. Brückner, S. Kroker, D. Friedrich, E.-B. Kley, and A. Tünnermann, Widely tunable monolithic narrowband grating filter for near-infrared radiation, Opt. Lett. **36**, 436 (2011).

[33] C.-T. Hsiung and C.-S. Huang, Refractive index sensor based on gradient waveguide thickness guided-mode resonance filter, IEEE Sens. Lett. **2**, 5001104 (2018).

[34] B. Sheng, H. Zhou, C. Tao, A. Zahid, Z. Ni, Y. Huang, R. Hong, and D. Zhang, Tunable and polarization-independent wedged resonance filter with 2D crossed grating, IEEE Photonics Technol. Lett. **28**, 2211 (2016).

[35] J.-M. Yang, N.-Z. Yang, C.-H. Chen, and C.-S. Huang, Gradient waveguide thickness guided-mode resonance biosensor, Sensors **21**, 376 (2021).

[36] G. J. Triggs, Y. Wang, C. P. Reardon, M. Fischer, G. J. O. Evans, and T. F. Krauss, Chirped guided-mode resonance biosensor, Optica **4**, 229 (2017).

[37] L. Qian, K. Wang, G. Wu, L. Zhu, C. Han, and C. Yan, Non-homogeneous composite GMR structure to realize increased filtering range, Opt. Express **26**, 23602 (2018).

[38] Y.-J. Hung, C.-W. Kao, T.-C. Kao, C.-W. Huang, J.-J. Lin, and C.-C. Yin, Optical spectrometer based on continuously-chirped guided mode resonance filter, Opt. Express **26**, 27515 (2018).

[39] N.-Z. Yang, C.-T. Hsiung, and C.-S. Huang, Biosensor based on two-dimensional gradient guided-mode resonance filter, Opt. Express **29**, 1320 (2021).

[40] Y. H. Ko, N. Gupta, and R. Magnusson, Resonant filters with concurrently tuned central wavelengths and sidebands, Opt. Lett. **45**, 6046 (2020).

[41] C. Fang, B. Dai, Z. Li, A. Zahid, Q. Wang, B. Sheng, and D. Zhang, Tunable guided-mode resonance filter with a gradient grating period fabricated by casting a stretched PDMS grating wedge, Opt. Lett. **41**, 5302 (2016).

[42] E. N. Ragozin, E. A. Vishnyakov, A. O. Kolesnikov, A. S. Pirozhkov, and A. N. Shatokhin, Soft X-ray spectrometers based on aperiodic reflection gratings and their application, Phys. Usp. **64**, 495 (2021).

[43] M. G. Moharam, E. B. Grann, D. A. Pommet, and T. K. Gaylord, Formulation for stable and efficient implementation of the rigorous coupled-wave analysis of binary gratings, J. Opt. Soc. Am. A **12**, 1068 (1995).

[44] L. Li, Formulation and comparison of two recursive matrix algorithms for modeling layered diffraction gratings, J. Opt. Soc. Am. A **13**, 1024 (1996).

[45] M. Pisarenco, J. Maubach, I. Setija, and R. Mattheij, Aperiodic Fourier modal method in contrast-field formulation for simulation of scattering from finite structures, J. Opt. Soc. Am. A **27**, 2423 (2010).

[46] M. Pisarenco, J. Maubach, I. Setija, and R. Mattheij, Modified S-matrix algorithm for the aperiodic Fourier modal method in contrast-field formulation, J. Opt. Soc. Am. A **28**, 1364 (2011).

[47] S. G. Tikhodeev, A. L. Yablonskii, E. A. Muljarov, N. A. Gippius, and T. Ishihara, Quasiguided modes and optical properties of photonic crystal slabs, Phys. Rev. B **66**, 045102 (2002).

[48] D. A. Bykov and L. L. Doskolovich, Numerical methods for calculating poles of the scattering matrix with applications in grating theory, J. Lightwave Technol. **31**, 793 (2013).

[49] D. A. Bykov and L. L. Doskolovich, Spatiotemporal coupled-mode theory of guided-mode resonant gratings, Opt. Express **23**, 19234 (2015).

[50] H. A. Haus, *Waves and Fields in Optoelectronics* (Prentice-Hall, Englewood Cliffs, NJ, 1984).